HySafe standard benchmark Problem SBEP-V11: Predictions of hydrogen release and dispersion from a CGH2 bus in an underpass

A.G. Venetsanos [a,*], E. Papanikolaou [a,d], O.R. Hansen [b], P. Middha [b], J. Garcia [c], M. Heitsch [d], D. Baraldi [d], P. Adams [e]

[a] Environmental Research Laboratory, National Centre for Scientific Research Demokritos (NCSRD), 15310 Aghia Paraskevi, Attikis, Greece
[b] GexCon AS, Fantoftvegen 38, Box 6015 Postterminalen, N-5892 Bergen, Norway
[c] Escuela Técnica Superior de Ingenieros Industriales, Universidad Politécnica de Madrid (UPM), José Gutiérrez Abascal, 2, E-28006 Madrid, Spain
[d] Joint Research Centre of the European Commission (JRC), Institute for Energy, 1755 ZG Petten, The Netherlands
[e] Volvo Technology Corp., Dept. 06120 Chalmers Teknikpark, 412 88 Gothenburg, Sweden

ARTICLE INFO

Keywords:
Hydrogen safety
Release and dispersion
CFD
Underpass
Tunnel
CGH2 bus

ABSTRACT

One of the tasks of the HySafe Network of Excellence was the evaluation of available CFD tools and models for dispersion and combustion in selected hydrogen release scenarios identified as "standard benchmark problems" (SBEPs). This paper presents the results of the HySafe standard benchmark problem SBEP-V11. The situation considered is a high pressure hydrogen jet release from a compressed gaseous hydrogen (CGH2) bus in an underpass. The bus considered is equipped with 8 cylinders of 5 kg hydrogen each at 35 MPa storage pressure. The underpass is assumed to be of the common beam and slab type construction with I-beams spanning across the highway at 3 m centres (normal to the bus), plus cross bracing between the main beams, and light armatures parallel to the bus direction. The main goal of the present work was to evaluate the role of obstructions on the underside of the bridge deck on the dispersion patterns and assess the potential for hydrogen accumulation. Four HySafe partners participated in this benchmark, with 4 different CFD codes, ADREA-HF, CFX, FLACS and FLUENT. Four scenarios were examined in total. In the base case scenario 20 kg of hydrogen was released in the basic geometry. In Sensitivity Test 1 the release position was moved so that the hydrogen jet could hit directly the light armature on the roof of the underpass. In Sensitivity Test 2 the underside of the bridge deck was flat. In Sensitivity Test 3 the release was from one cylinder instead of four (5 kg instead of 20). The paper compares the results predicted by the four different computational approaches and attempts to identify the reasons for observed disagreements. The paper also concludes on the effects of the obstructions on the underside of the bridge deck.

1. Introduction

Within the framework of assessing the risk of hypothetical hydrogen releases from hydrogen vehicles, various environments have to be considered, e.g. urban, tunnels, garage etc. One of these environments could be an underpass below a highway. A related accident involving a petrol tanker under a bridge happened in San Francisco, USA recently (San-Francisco [12] and according to the reporters the "huge leaping flames from the exploding gasoline tanker melted the steel underbelly of the highway overpass, causing it to collapse onto the roadway below virtually ensuring major traffic problems".

As to the authors' knowledge previous hydrogen safety related work on an underpass does not exist, but the previous work on tunnels is briefly reviewed given that there are strong similarities between an underpass and a tunnel. Earlier (and current) studies of hydrogen releases in tunnels include the work of Wilkening et al. [17], Venetsanos et al. [13], Middha and Hansen [9], Kumar et al. [7], Mukai et al. [11] and Baraldi et al. [2].

Wilkening et al. [17] considered hydrogen releases from a compressed gaseous hydrogen (CGH2) and liquefied hydrogen (LH2) car within a 200 m tunnel of horseshoe cross section within the EIHP project (www.eihp.org). Later, Venetsanos et al. [13] used the same tunnel geometry and investigated hydrogen and natural gas releases from a CGH2 and compressed natural gas (CNG) bus within the EIHP-2 project (www.eihp.org). In both studies only one car or one bus was involved and no other vehicles were assumed to be present. Later, in the work performed within the HyTunnel internal project of HySafe NoE (www.hysafe.net) the previous studies were extended by considering the same tunnel cross section but assuming a rush hour with many vehicles present along the tunnel on both sides. The HyTunnel project also considered a tunnel with flat roof and approximately the same cross sectional area in order to investigate the effect of the roof geometry.

What the above mentioned studies did not examine was the presence of various obstacles along the tunnel roof. Such obstacles can affect the dynamics of both hydrogen (and natural gas) dispersion and combustion and the extreme case is an underpass with beam and slab construction of the type considered in this paper. If the geometry is appropriate, flammable hydrogen can be trapped within the roof structures and remain there for a long time and thus increase the risk associated with an accidental release significantly. However, the ventilation in underpasses would typically be much better than in longer tunnels. In case of the flammable mixture being ignited the presence of obstacles could enhance acceleration and turbulence production, parameters which can both lead to a transition to a fast deflagration or DDT (deflagration to detonation transition).

Within the above framework, the focus of the present work was two-fold: to investigate the effects of the roof obstructions and at the same time to examine the variation between different partners' predictions.

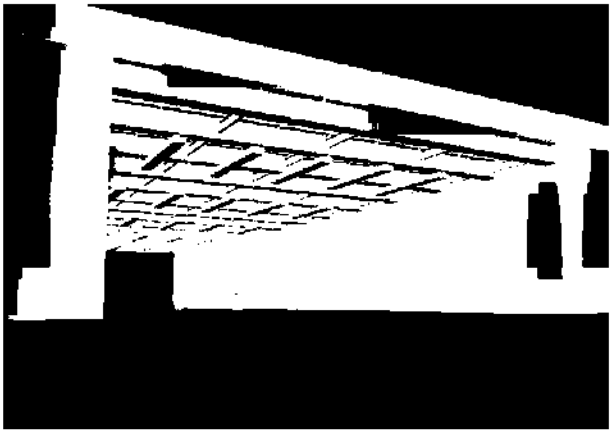

Fig. 1 – Geometry. I beams (in red), cross bracing and stiffeners (in blue), light armature (in yellow).
(For interpretation of the references to colour in this figure legend, the reader is referred to the web version of this article.)

2. SBEP-V11 specifications

The situation considered is a hydrogen release from a stationary bus in an underpass (see Fig. 1). Ambient conditions are quiescent with 15 °C temperature and 1 bar pressure. No other vehicles are assumed to be present except for the hydrogen bus. It is assumed that the bus remains upright after the incident (and at the same position).

The underpass is assumed to be of the common beam and slab type and construction with I-beams spanning across the highway. The underpass has a span of 15 m (X) length of 42 m (Y) and height 6 m (Z) (to the underside of bridge deck). There are 0.8 m (Z-depth) I-beams at 3 m centres in Y direction (1 cm Y-thick web with 50 cm Y-ends) (in red, see Fig. 1). Each I-beam has stiffeners on both sides of the web at the cross bracing positions and mid-way between the braces (in blue). There are also 0.3 m deep cross bracings between the beams at supports, mid-span, and quarter-span (in blue). Finally there are light armatures: 4 m (Y) × 0.4 m (X) × 0.2 m (Z) located at a height of 5 m (in yellow). The armature units are located every 2.5 m in the span (X) direction of the underpass (with first one at 2.3 m) and every 8 m along the highway (Y) direction (with first one at 3 m).

The bus has width 2.55 m (X), length 12 m (Y), height to top of tanks 3.2 m (Z) and 30 cm spacing under the bus (the wheels are 80 cm diameter and 40 cm thick (X)). The lower left corner of the bus is located at horizontal position 8 m (X) and 10 m (Y) (origin 0, 0, 0 is at the underpass corner).

The bus is assumed equipped with an eight cylinder storage system at 35 MPa (two banks of four interconnected cylinders) as in Venetsanos et al. [13] containing in total 40 kg of hydrogen. Each cylinder is equipped with two pressure relief devices (PRDs) according to regulations. The PRD nozzle diameter is assumed to be 4 mm. Each group of four neighbouring PRDs are vented into a 20 mm vent line. There are in total four such outlet vent lines.

Four scenarios were examined in total, the base case and three sensitivity tests.

- In the base case scenario the underpass geometry (basic geometry) is as described above. For this scenario it is

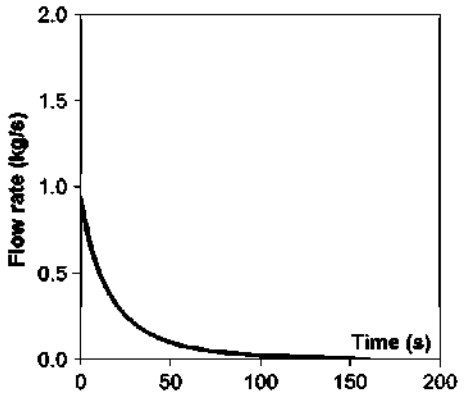

Fig. 2 – Predicted mass flow rate for 20 kg hydrogen release at 35 MPa, ambient temperature from 4×4 mm diameter nozzles.

assumed that we have simultaneous opening of the 4 PRDs that feed one of the outlet lines, which is located at position 9 m, 20 m, 3.3 m, resulting in an upwards directed jet and release of 20 kg of hydrogen, which is the inventory of four cylinders.

- In Sensitivity Test 1 the release position was modified such that the hydrogen jet hits the light armature (release position 10 m, 20 m, 3.3 m). All other parameters were as in the base case.
- In Sensitivity Test 2 the underside of the bridge deck at $Z = 5$ m was flat (sensors are moved to 4.8 m, see below). All other parameters were as in the base case.
- For Sensitivity Test 3 it was assumed that only one PRD was activated so only 5 kg of hydrogen (1 tank) were released. All other parameters were as in the base case.

The leak rate was calculated by NCSRD using the GAJET integral code, as shown in Fig. 2. The calculation was performed for 1 cylinder (5 kg hydrogen) with 4 mm nozzle, real gas hydrogen properties and discharge coefficient 0.8. The rate was multiplied by 4 (effective nozzle diameter 8 mm) in case of the 4 cylinders release. The leak rate calculated by NCSRD was also applied by UPM and GexCon. JRC followed a different approach as explained in section 3.2 below, but which led to practically the same mass flow rate curve as with the other partners.

The hydrogen concentrations (v/v) are reported in this SBEP at 10 monitor points (sensors) located every 4 m along the Y direction starting at $X = 7.5$ m, $Z = 5.8$ m and $Y = 3$ m. Also reported (optional) were the flammable volume and the equivalent stoichiometric cloud volume $Q9 = \sum(V \times U_{bl} \times E)/(U_{bl} \times E)_{stoich}$ [9] as a function of time. Here, V is the flammable volume, U_{bl} is the laminar burning velocity (corrected for flame wrinkling/Lewis number effects), E is volume expansion caused by burning at constant pressure in air, and the summation is over all control volumes. Thus, Q9 cloud is a scaling of the non-homogeneous gas cloud to a smaller stoichiometric gas cloud with scaling parameters the expansion and the reactivity.

3. Modelling strategy

The modelling options used by each partner are summarized in Tables 1 and 2. Details for each partner are given below.

3.1. GexCon

GexCon has used the FLACS code. Earlier validation work for hydrogen dispersion is summarized in Middha et al. [10]. FLACS uses a standard k-ϵ model for turbulence. Some modifications are however implemented [1,6]. These are, for example (a) the model for generation of turbulence behind sub-grid objects, (b) the model for the build-up of proper turbulence behind objects of a particular size for which the discretization produce too little turbulence, (c) the turbulent wall functions, (d) the buoyancy generated turbulence and (e) the initial turbulence/inflow field calculated from Pasquill class.

A structured Cartesian grid was used. The default grid resolution was 50 cm, and the grid was refined near the hydrogen release and near the ceiling as stratification was expected. The total number of cells ranged from about 240,000 to 340,000 depending on the release rate (one cylinder or four cylinder release) and the geometry (flat or with beams). The

Table 1 – Summary of modelling options by each partner.

Partner	Domain	Min cell	Grid	Source (four cylinders)	Turbulence model	Discretization schemes
GexCon	35 × 72 × 14 m	13 cm horiz, 25 cm vert	294,063 cells	Initial fict. diam. 13.5 cm	Standard k-eps with buoyancy effects and additional turbulence generation behind objects of a particular size	Second order Kappa schemes
NCSRD	45 × 70 × 15 m	10 cm	245,622 cells	Birch et al. [3], Initial fict. diam. 10.4 cm	Standard k-eps with buoyancy effects	First order upwind, Time steps $1e^{-6}$-0.1
JRC	100 m diameter, 38 m height	~1 mm	264,264 nodes, 12,98,267 cells (tetrahedrons, prisms and pyramids)	No fict. diam., Storage cylinder and 8 mm nozzle included in calculations	SST	Second order accurate
UPM	15 × 62 × 9 m	1.5 cm	660,000 cells for the base case and 193,000 for the sensitivity cases	Birch et al. [3], Initial fict. diam. 10.4 cm	Standard k-eps with buoyancy effects	Third order MUSCL scheme, time steps 0.01–0.1 s

Table 2 – Boundary and initial conditions by each partner.

Partner	Walls and ground	Free domain	Source	Initialization
GexCon	Wall functions for velocity, turbulent kinetic energy, dissipation rate and enthalpy. Smooth ground	Constant pressure planes for normal velocity components. For scalar variables and tangential velocity components zero gradient if outflow or initial value (at time 0) if inflow	Subsonic velocity (after shock). Atmospheric pressure. Temperature 288 K. Time varying source area. Turbulent intensity 0.2 and Turbulent length scale 10% of expanded diameter	Zero velocities. Atmospheric pressure. Ambient temperature 288 K. Turbulent kinetic energy 1e $^{-3}$ m^2/s^2
NCSRD	Wall functions for velocity, turbulent kinetic energy and dissipation rate. Hydrodynamic roughness 1 mm	Constant pressure planes (pressure hydrostatic) for normal velocity components. For scalar variables and tangential velocity components zero gradient if outflow or initial value (at time 0) if inflow	Sonic velocity. Atmospheric pressure. Temperature 288 K. Time varying source area. Zero turbulent kinetic energy. Zero diffusion	Zero velocities. Hydrostatic pressure. Ambient temperature 288 K. Turbulent kinetic energy 1e^{-5} m^2/s^2
JRC	Wall functions	In a distance of about 30 m from the tunnel vertical walls were placed. 30 m above the tunnel a large opening (flow in both directions) was defined	Hydrogen tank included in the mesh. Leak flow calculated from pressure difference between tank and environment without further assumptions. Real gas (Redlich Kwong) behaviour applied for hydrogen (35 MPa in tank).	Zero velocities. 1 bar air pressure. Ambient temperature 288 K. Turbulent kinetic 1e^{-4} m^2/s^2 and dissipation 1e^{-4} m^2/s^3
UPM	Wall functions	Ambient pressure (1 bar) for open boundaries	Birch approximation: sonic velocity and ambient pressure. Source area variable with time. Zero turbulent kinetic energy	Zero velocities and turbulent kinetic energy. Ambient pressure (1 bar) and temperature (288 K)

grid was extended outside the underpass to have the boundary at the appropriate distance, in order to reduce the effect of the boundary conditions on the calculations.

Second order schemes (Kappa schemes with weighting between second order upwind and second order difference, delimiters for some equations) were used.

3.2. JRC

JRC used the CFX 11 SP1 code. Earlier related validation work using CFX can be found in [5,16]. In the present calculations turbulence was modelled using the SST turbulence model of CFX with buoyancy terms for production and dissipation being activated. For both the convective and the temporal terms second order accurate schemes were applied.

Around the underpass a large hemispherical volume (environment) was placed as outer boundary of the computational domain. A large size was chosen in order to reduce the effect of the boundary conditions on the simulations. The outer surfaces of the computational domain were defined mainly as walls and only the uppermost part of the domain was defined as outlet which allows only flow out of the domain. By these means the formation of an artificial flow through the underpass was avoided. The mesh created for the base case included 264264 nodes or 1298267 cells (tetrahedrons, prisms and pyramids).

The leak in the tank of the bus was calculated directly and not simulated by the Birch approach. A properly sized cylindrical volume (either representing four or one cylinders) was placed inside the bus combined with an outflow pipe of 8 mm (cross-section equivalent to four pipes of 4 mm diameter) or 4 mm diameter at the given leak position. The flow through the leak was then calculated from the time varying pressure difference between tank and flow domain starting from the given initial tank pressure. Real gas conditions according to the Redlich–Kwong EoS were applied. The tank in the bus was dimensioned to contain 20 or 5 kg hydrogen (35 MPa, 15 °C) at the beginning of the simulation.

Sufficiently small time steps together with a mesh refinement in the jet region were necessary to simulate the under expanded jet released from the high pressure tank. The calculated maximum jet velocities downstream of the leak were in the order of 2700 m/s. The resulting high momentum in the jet improved the gas mixing in the underpass around the bus considerably. Consequently hydrogen concentrations at monitor positions as discussed in the following paragraphs are often lower and more uniform than obtained by the Birch approach of the other partners.

3.3. NCSRD

NCSRD has used the ADREA-HF code. Earlier validation work using ADREA-HF code has been summarized in Venetsanos et al. [14]. The mixing of H_2 with air was calculated by solving the three dimensional transient, fully compressible conservation equations for mixture mass (continuity equation), mixture momentum (for the three velocity components) and the H_2 mass fraction transport equation. Turbulence was modelled using the two equation standard k–ϵ model of Launder and Spalding [8], modified for buoyancy effects.

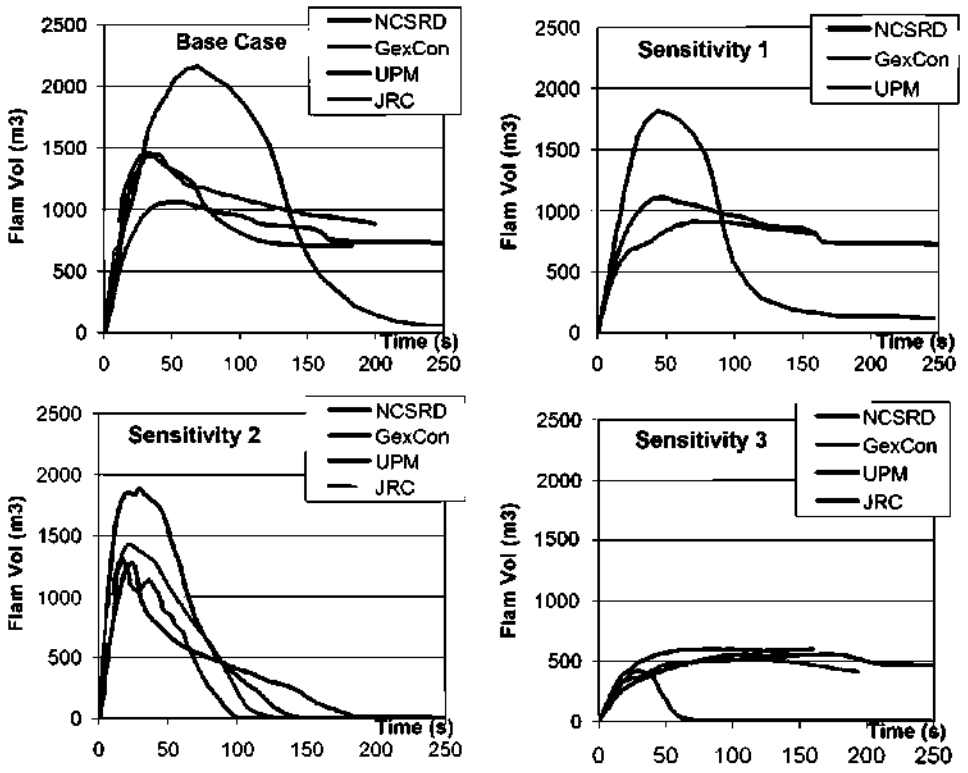

Fig. 3 – Predicted flammable mixture volume (m^3) histories per scenario case. Base case scenario: 20 kg of hydrogen was released in the basic geometry. Sensitivity Test 1: the hydrogen jet was moved to hit the light armature. Sensitivity Test 2: the underside of the bridge deck was flat. Sensitivity Test 3: the release was from one cylinder instead of four (5 kg instead of 20 kg).

The computational domain extended the borders of the underpass by 20 m in the Y direction by 15 m in the X-direction and by 15 m in the Z-direction. The computational grid is a non-uniform Cartesian grid consisting of $68 \times 78 \times 47$ (245622) cells. Minimum cell size is 0.1 m in all three directions located at the source. This was kept constant for a region up to 0.5 m from the source. Further away a grid expansion of 1.12 was used. The presence of solids within the rectangular grid was treated with the volume porosity and area permeability approach.

Initial conditions at the source were set according to the Birch et al. [3] approach, i.e. sonic velocity (assumed to be 1294 m/s), atmospheric pressure and ambient temperature of 288 K. The source diameter varied in time (0–154 s) to get the flow rate given in Fig. 2. Initial fictitious diameter was approximately 10.4 cm for the four cylinders case and 5.2 cm for the one cylinder case.

The numerical options used were the first order fully implicit scheme for time integration and the first order upwind scheme for the discretization of the convective terms. The increase of the time step was bounded by applying simultaneously two restrictions a maximum allowed time step of 0.1 seconds and a maximum convective CFL number of 2.

3.4. UPM

UPM has used the Fluent 6.2 code. Earlier validation using Fluent can be found in [4] and [15]. In the present simulations turbulence was modelled using the standard k–ϵ model. The SIMPLE method was employed and a third order MUSCL scheme was used for the convective scheme. A fixed time stepping method was used ranging from 0.01 to 0.1 s.

A structured hexahedral mesh was used. The number of cells was 660,000 for the base case and Sensitivity Cases 1 and 3. For Sensitivity Case 2 the grid is the same but without the upper part corresponding to $z > 5$ m, resulting in a mesh of 193,000 cells. The grid was refined near the H_2 release (the minimum cell size was 1.5 cm).

4. Results and discussion

As mentioned above the objectives of the SBEP were twofold: to examine the effect of the presence of the obstructions such as I-beams in the roof of the structure and to compare the variations between different partner predictions. In the discussion below the predictions obtained by different partners are compared first.

One of the parameters used in assessing the risk of an accidental release is the flammable mixture volume, i.e. the volume of the hydrogen-air mixture, where hydrogen concentration is within the lower and upper flammability limits (4–75% respectively). The predicted flammable mixture volumes by each participant as a function of time are shown in Fig. 3 for the four cases considered (base plus three sensitivity cases). It can be observed that there are similarities but also significant differences in some cases between different predictions, especially

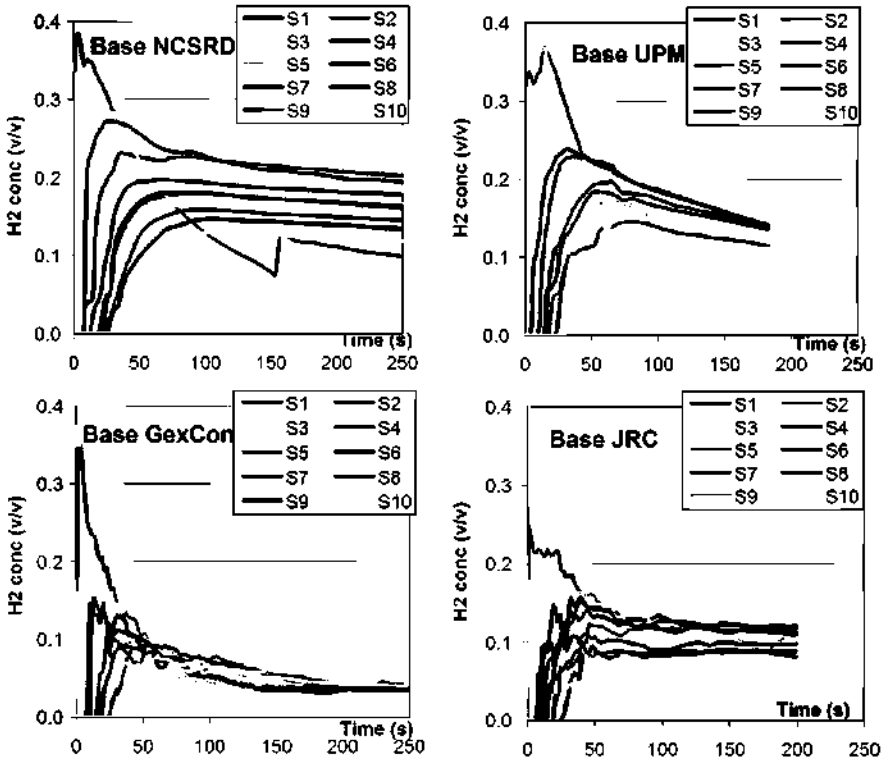

Fig. 4 – Base case: predicted hydrogen concentration time histories at sensors (1–10) locations.

regarding the size of the maximum predicted flammable volume, the time of its occurrence as well as the behaviour of the flammable volume history at and beyond the end of the release.

More specifically, for the base case and Sensitivity Tests 1 and 3, the UPM, NCSRD and JRC predictions show a similarity as they predict nearly the same flammable volume at large times, while the difference in predicted maximums is not so pronounced. On the other hand, GexCon predicts a different behaviour with small flammable volume values at large times for all the above cases and much higher maximum flammable volume for the base case and Sensitivity Test 1. For Sensitivity Test 2 on the other hand, despite the differences in predicted maximum flammable volume, it seems that there is general agreement in predicted behaviour between all four participants.

The above shows a general agreement between predictions when the underside of the bridge deck is flat (Sensitivity Test 2), and deviations when the underside of the bridge deck includes the I-beams (base case, Sensitivity Tests 1 and 3). In the later case two different behaviours occur at large times: UPM, JRC

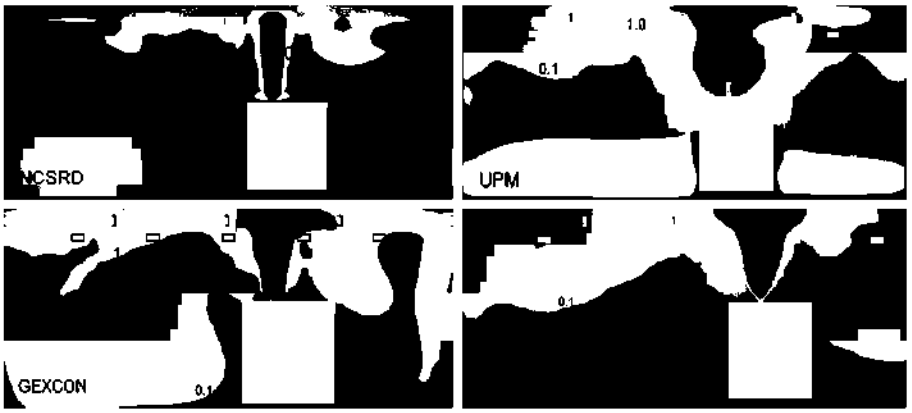

Fig. 5 – Base case: Turbulent kinetic energy predictions on the XZ vertical plane through the source at time 40 s. Colours: blue (< 0.1), green (0.1–1.0), yellow (1.0–10), red (> 10). (For interpretation of the references to colour in this figure legend, the reader is referred to the web version of this article.)

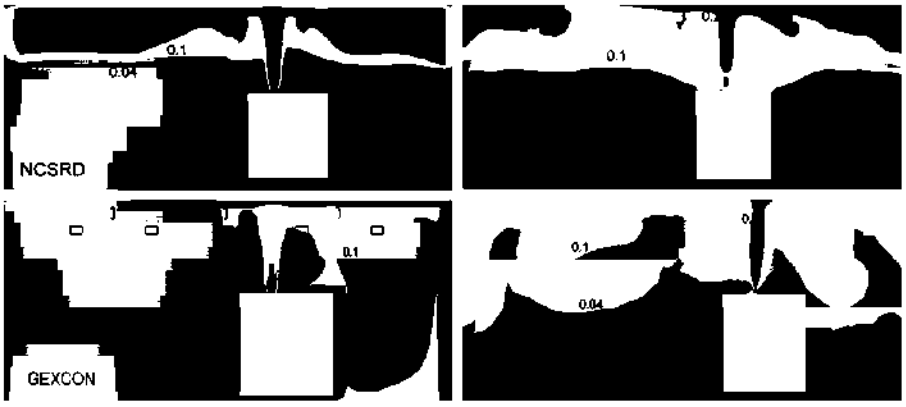

Fig. 6 – Base case: hydrogen concentration (v/v) predictions on the XZ vertical plane through the source at time 50 s. Colours: blue (< 0.04), green (0.04–0.1), yellow (0.1–0.2), red (> 0.2). (For interpretation of the references to colour in this figure legend, the reader is referred to the web version of this article.)

and NCSRD predict large flammable hydrogen values near and after the end of the release while GexCon predicts flammable hydrogen disappearing.

The above mentioned behaviour is re-examined below in the light of the predicted hydrogen concentration time histories at the selected sensor locations. Fig. 4 shows the predicted concentration time histories per partner for the base case scenario. For all partners the highest concentration is observed for sensor 5, located at Y = 19 m, which is the closest to the source. Next in magnitude are sensors 4 and 6 located south and north from the source at Y = 15 and Y = 23 m followed by sensors 3 and 7 and so on. The earlier mentioned similarity between NCSRD, JRC and UPM can also be observed here. The concentration values at large times are between 10 and 20% for NCSRD and UPM and down to 7% for JRC. On the other hand the corresponding concentrations as predicted by GexCon are less than the lower flammability limit of hydrogen (4%), which is consistent with the behaviour observed in Fig. 3.

Predicted hydrogen concentration histories for Sensitivity Test 2 (flat roof at Z = 5 m) are presented in Fig. 7 below to be compared with Fig. 4 for the base case. It can be observed that the concentrations predicted by all the partners are of similar

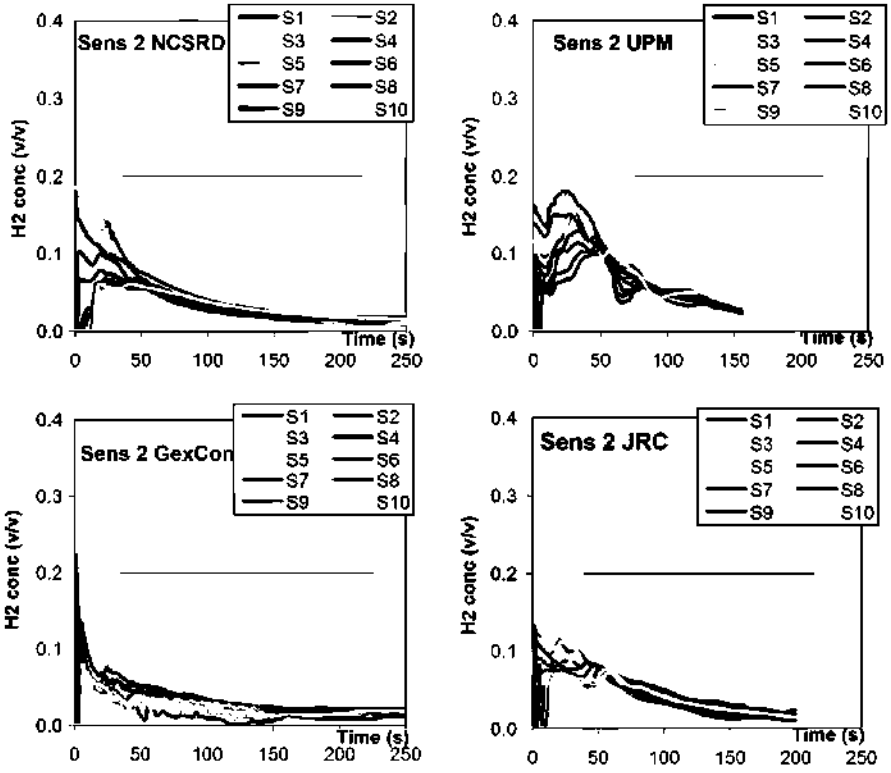

Fig. 7 – Sensitivity test 2 (flat roof at z = 5 m): predicted hydrogen concentration time histories at sensors (1–10) locations.

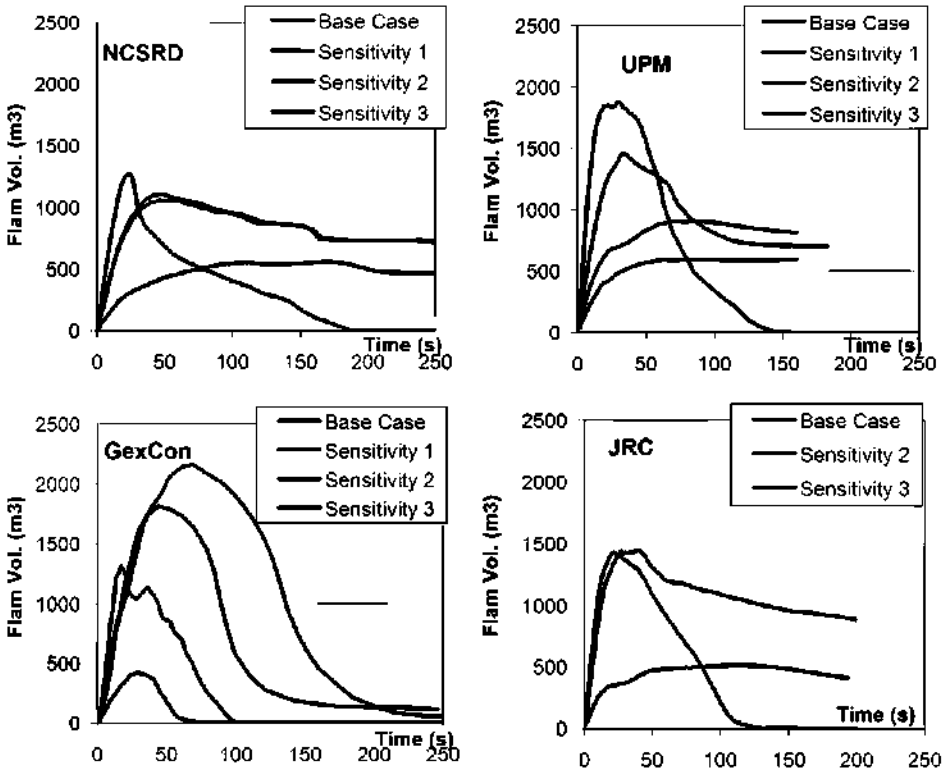

Fig. 8 – Predicted flammable mixture volume (m^3) histories per partner.

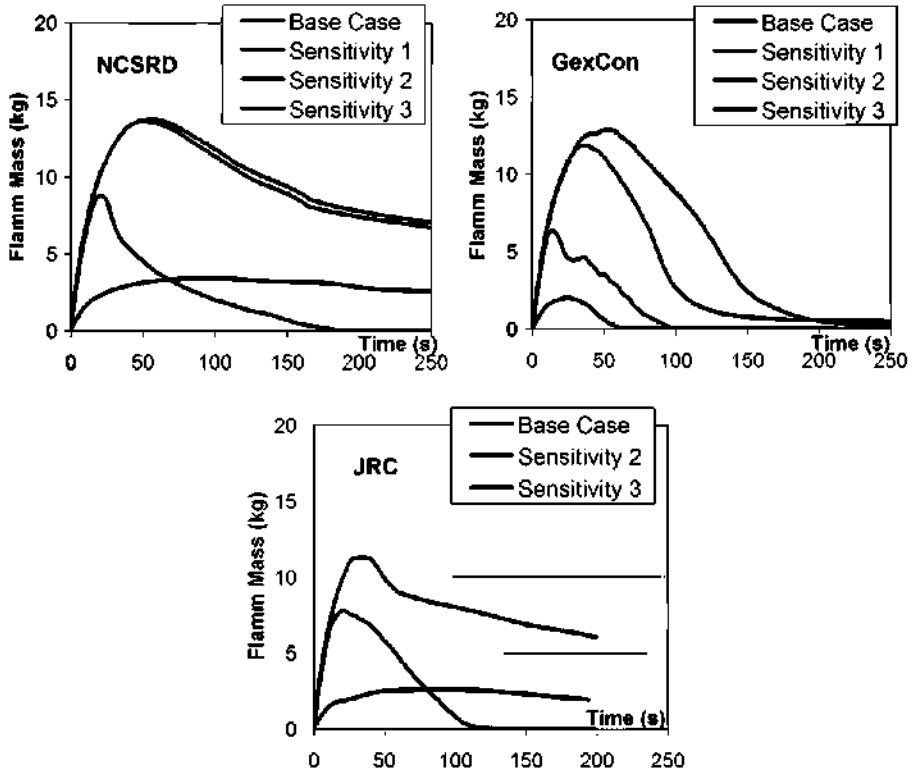

Fig. 9 – Flammable hydrogen mass predictions.

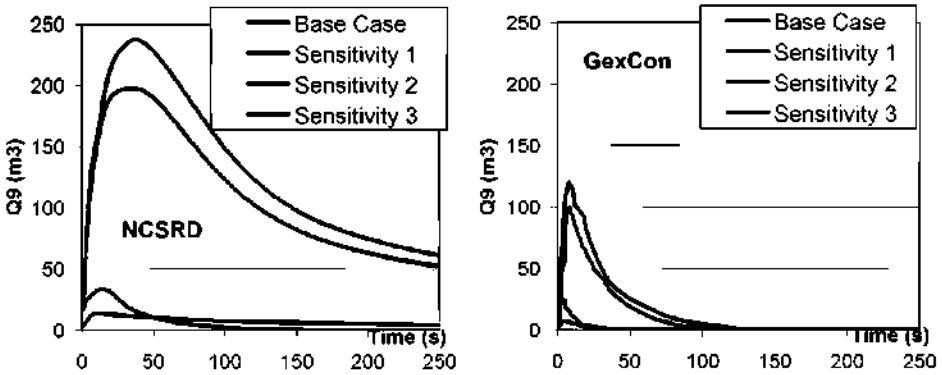

Fig. 10 – Equivalent stoichiometric cloud volume (Q9) predictions.

levels, which is consistent with the similarity observed for the predicted flammable volumes in Fig. 3. It can also be observed that concentration levels are lower than for the base case due to hydrogen accumulation effects within the I-beams.

The lower level of concentrations predicted by GexCon in Fig. 4 compared to the other partners can be attributed to higher levels of turbulent mixing. This is shown in Fig. 5, which presents the predicted turbulent kinetic energy field for each partner on the XZ plane through the source at time 40 s. This increased turbulent mixing for GexCon is responsible both for the larger maximum flammable volume and for the much lower flammable volume at large times. Increased mixing leads in general to an increased cloud size but with lower concentrations. So increased mixing in a region of high concentrations can lead to an increase in the volume of the flammable cloud if the concentrations do not drop below the lower flammability limit, while increased mixing in a region of low concentrations can lead to the disappearance of the flammable cloud if concentrations drop below the LFL. A comparison of the predicted concentration field for each partner on the XZ plane through the source at time 50 s is shown in Fig. 6. It can be observed that the GexCon flammable cloud covers most of the underpass cross-section.

Regarding the source of this increased mixing for GexCon, it should be noted that the difference between GexCon and the other predictions occurs when the I-beams are present and not in case where the underside of the bridge deck is flat (Sensitivity Test 2), so a logical explanation could be to attribute the above mentioned increased turbulence levels to the modelling of the roof structures. Along this line, as mentioned in Section 3.1, GexCon uses a model for generation of turbulence behind sub-grid objects and a model for build-up of proper turbulence behind objects of a particular size for which the discretization produces too little turbulence. The effect of these models could be the reason for the above mentioned increased turbulence levels.

It can also be seen from Fig. 4 that there is a sudden increase (kink) in the NCSRD concentration trace for sensor 5 at around 150 s and a nearly similar kink in the UPM concentration at approximately 60 s. It can also be observed that for NCSRD the concentrations at this location (nearest the source) become the lowest predicted concentrations at around 100 s. The low hydrogen concentration predicted close to the source (sensor 5) compared to sensors further away is not unreasonable, since the leak rate at 100 s is very low (0.02 kg/s) compared to the beginning of the leak (approx 0.9 kg/s). The increase in hydrogen concentration at sensor 5 is associated to hydrogen re-approaching the source after being transported and accumulated far from it. The sudden increase could be associated with an obstacle effect, i.e. hydrogen suddenly passing over an obstacle (cross-bracings). The JRC prediction for sensor 5 shows an effect similar to NCSRD and UPM, but this effect is only seen at the very end of the outflow (around 170 s). Shortly before this time the concentration at sensor 5 drops below the concentrations at the neighbouring monitor locations. When the flow stops the trapped hydrogen mixes with the surroundings and the concentration at sensor 5 grows slowly. GexCon prediction does not show a similar phenomenon. The difference between partners' predictions regarding the above concentration increase could be attributed to the different turbulence modelling schemes used. More insight is needed on this special effect in the future.

The results of the performed sensitivity tests are reported below. Fig. 8 shows the predicted flammable volumes per partner. NCSRD and UPM predictions show a similarity. With the given roof obstructions (base case) the max flammable volume is decreased and a large flammable volume is preserved up to and beyond the end of release compared to Sensitivity Test 2. JRC predictions agree with NCSRD and UPM as far as the behaviour at large times. For the maximum flammable volume JRC predictions show that it remains practically unchanged. GexCon's prediction on the other hand shows a different behaviour. The maximum flammable volume is significantly increased with the I-beams and is reduced considerably after the end of release. This is associated with the increased mixing as mentioned above.

The very important effect of the I-beam structure compared to the flat roof is presented in Fig. 9 which shows the predicted flammable mass histories. In the base case there is an increase of the maximum flammable mass with respect to the flat roof (Sensitivity Test 2) by 57% according to NCSRD, 45% according to JRC and 105% according to GexCon, the absolute values being 13.8, 11.3 and 12.8 kg, respectively. A similar and even more pronounced picture is presented in Fig. 10 which shows the equivalent stoichiometric cloud volume histories. With I-beams the maximum Q9 is increased

from approximately 25–30 m^3 with flat roof to 240 m^3 (NCSRD) and 120 m^3 (GexCon).

The effect of hitting the light armature was investigated in Sensitivity Test 1. Fig. 8 shows that both GexCon and UPM predict lower flammable volume in this case as compared to the base case. NCSRD on the other hand did not see any important difference. Regarding the effect of releasing the contents of only one cylinder instead of four (5 kg instead of 20 kg) in the initial geometry, Fig. 8 shows that the flammable volumes are lower in all cases as expected.

5. Conclusions

Within the framework of HySafe NoE, co-funded by the EC, four HySafe partners performed CFD flow and dispersion calculations for benchmark SBEP-V11 with four different CFD codes, ADREA-HF, CFX, FLACS and FLUENT to simulate a hydrogen release from a bus in an underpass. The underpass is assumed to be of the common beam and slab type and construction with I-beams spanning across the highway at 3 m centres plus cross bracing and light armatures creating cavities where hydrogen could potentially accumulate. Four scenarios were examined in total. For the base case the release was vertically upwards from one outlet fed from four cylinders containing in total 20 kg of hydrogen at 35 MPa. In Sensitivity Test 1 the source was horizontally moved so that the vertical hydrogen jet hit the light armature before reaching the roof. In Sensitivity Test 2 the underside of the bridge deck was entirely flat. In Sensitivity Test 3 only 5 kg of hydrogen were released instead of 20 kg in the base case geometry. The performed simulations led to the following conclusions:

- Comparison between partners' predictions for the flammable volume history showed that there is general agreement when the underside of the bridge deck is flat (Sensitivity Test 2) and deviations when the I-beams are included (base case, Sensitivity Tests 1 and 3). In the later cases two different behaviours were observed at large times: NCSRD, JRC and UPM predict large flammable hydrogen values near and after the end of the release while GexCon predicts flammable hydrogen disappearing. The behaviour as predicted by GexCon was attributed to larger turbulent mixing, caused by the modelling of additional turbulence behind obstacles of a particular size.
- The presence of the I-beams leads to higher hydrogen concentrations, due to hydrogen-air cloud accumulation within the cavities. This was confirmed by all participating partners. Flammable volume behaviour on the other hand was found to have different trends. NCSRD and UPM found a lower maximum flammable volume with I-beams and large values persisting near and after the end of the release, while GexCon calculated a higher maximum and values falling to zero after the end of the release. For JRC the maximum was not affected by the presence of the beams, but the behaviour at large times was similar to UPM and NCSRD. The maximum appears early in the transient; at that time hydrogen is still concentrated in the jet region. According to the JRC simulation the mixing is dominated by the momentum of the jet and therefore the presence of I-beams is not important for the maximum size of the flammable cloud.
- The effect of the I-beam structure compared to the flat roof was found to be very important. In the base case there is an increase of the maximum flammable mass with respect to the flat roof (Sensitivity Test 2) by 57% according to NCSRD, 45% according to JRC and 105% according to GexCon, the absolute values being 13.8, 11.3 and 12.8 kg, respectively. Additionally with I-beams the max Q9 are increased from approximately 25–30 m^3 (both NCSRD and GexCon) with flat roof to 240 m^3 (NCSRD) and 120 m^3 (GexCon).
- The change in the release position such that the jet hits the light armature (Sensitivity Test 1) leads to decreased flammable volumes according to GexCon and UPM, while the effect was negligible for NCSRD.
- As expected the reduction of released mass wherein the contents of only one cylinder instead of four (5 kg instead of 20 kg) were emptied in the base geometry (Sensitivity Test 3), led to significantly lower flammable volumes in the simulations of all partners.
- Finally, the variation between the different models clearly demonstrates the need to further validate CFD models for the observed phenomena by conducting experiments representative of the environment and range of conditions examined within this study.

Acknowledgements

Despite the non-existence of experimental data this work was considered very valuable and was therefore proposed and performed as SBEP-V11 (Standard Benchmark Exercise Problem) of the HySafe NoE project co-funded by the EC, which the authors gratefully acknowledge.

REFERENCES

[1] Arntzen BA. Modeling of turbulence and combustion for simulation of gas explosions in complex geometries. PhD Thesis, NTNU, Trondheim, Norway; 1998.
[2] Baraldi D, Kotchourko A, Lelyakin A, Yanez J, Middha P, Hansen OR, et al. An inter-comparison exercise on CFD model capabilities to simulate hydrogen deflagrations in a tunnel. Int J Hydrogen Energy 2009;34:7862–72.
[3] Birch AD, Brown DR, Dodson MG, Swaffield F. The structure and concentration decay of high pressure jets of natural gas. Combust Sci Technol 1984;36:249–61.
[4] Gallego E, Migoya E, Martin-Valdepenas JM, Crespo A, Garcia J, Venetsanos AG, et al. An intercomparison exercise on the capabilities of CFD models to predict distribution and mixing of H_2 in a closed vessel. Int J Hydrogen Energy 2007; 32(13):2235–45.
[5] Heitsch M, Baraldi D, Wilkening H. Simulation of containment jet flows including condensation. Grenoble: OECD-XCFD4NRS Workshop; 2008.
[6] Hjertager BH, Solberg T. A review of computational fluid dynamics (CFD) modeling of gas explosions. In: Zarko VE, editor. Prevention of hazardous fires and explosions. Kluwer Academic Publishers; 1999. p. 77–91.
[7] Kumar S, Miles S, Adams P, Zenner M, Ledin S, Kotchourko A, et al. HyTunnel: the use of hydrogen road

vehicles in tunnels. In: Third International Conference on Hydrogen Safety, Ajaccio, Corsica, France; 16–18 September 2009.
[8] Launder BE, Spalding DB. The numerical computation of turbulent flows. Comput Methods Appl Mech Eng 1974;3(2): 269–89.
[9] Middha P, Hansen OR. CFD simulation study to investigate the risk from hydrogen vehicles in tunnels. Int J Hydrogen Energy 2009;34(14):5875–86.
[10] Middha P, Hansen OR, Storvik IE. Validation of CFD-model for hydrogen dispersion. J Loss Prevent Proc Ind 2009;22(6): 1034–8.
[11] Mukai S, Suzuki J, Mitsuishi H, Oyakawa K, Watanabe S. CFD simulation of diffusion of hydrogen leakage caused by fuel cell vehicle accident in tunnel, underground parking lot and multi-story parking garage. In: 19th International Technical Conference on the Enhanced Safety of Vehicles (ESV), Washington, D.C.; June 6–9 2005.
[12] San-Francisco Chronicle. Tanker fire destroys part of MacArthur Maze; 2007. Available from: http://www.sfgate.com/cgi-bin/article.cgi?f=/c/a/2007/04/29/BAGVOPHQU46.DTL.
[13] Venetsanos AG, Baraldi D, Adams P, Heggem PS, Wilkening H. CFD modelling of hydrogen release, dispersion and combustion for automotive scenarios. J Loss Prevent Proc 2008;21:162–84.
[14] Venetsanos AG, Papanikolaou E, Bartzis JG. The ADREA-HF CFD code for consequence assessment of hydrogen applications. Int J Hydrogen Energy 2010;35(8): 3908–18.
[15] Venetsanos AG, Papanikolaou E, Delichatsios M, Garcia J, Hansen OR, Heitsch M, et al. An inter-comparison exercise on the capabilities of CFD models to predict the short and long term distribution and mixing of hydrogen in a garage. Int J Hydrogen Energy 2009b;34(14):5912–23.
[16] Wilkening H, Baraldi D, Heitsch M. CFD simulations of light gas release and mixing in the Battelle experimental facility with CFX. Nuclear Eng Des 2008;238:618–26.
[17] Wilkening H, Venetsanos AG, Huld T, Bartzis JG. Safety assessment of hydrogen as a fuel for vehicles by numerical simulation. Euro-conference on new and renewable technologies for sustainable development, Madeira Island, Portugal; 26–29 June 2000.